Fram Strait sea ice outflow

R. Kwok, G. F. Cunningham, and S. S. Pang
Jet Propulsion Laboratory, California Institute of Technology, Pasadena, California, USA

Received 15 January 2003; revised 2 July 2003; accepted 27 October 2003; published 6 January 2004.

[1] We summarize 24 years (1978–2002) of ice export estimates and examine, over a 9-year record, the associated variability in the time-varying upward-looking sonar (ULS) thickness distributions of the Fram Strait. A more thorough assessment of the PMW (passive microwave) ice motion with 5 years of synthetic aperture radar (SAR) observations shows the uncertainties to be consistent with that found by *Kwok and Rothrock* [1999], giving greater confidence to the record of ice flux calculations. Interesting details of the cross-strait motion profiles and ice cover characteristics revealed by high-resolution SAR imagery are discussed. The average annual ice area flux over the period is 866,000 km^2/yr. Between the 1980s and 1990s, the decadal difference in the net exported ice area is ~400,000 km^2, approximately half the annual average. Except for the years with extreme negative NAO, correlation of winter ice area export with the NAO index remains high ($R^2 = 0.62$). With thickness estimates from ULS moorings, we estimate the average annual ice volume flux (8 years) to be ~2218 km^3/yr (~0.07 Sv). Over the ~9-year ULS ice thickness data set, there is an overall decrease of 0.45 m in the mean ice thickness over the entire time series and a decrease of 0.23 m over the winter months (December through March). Correspondingly, the mode of the MY ice thickness exhibits an overall decrease of 0.55 m and a winter decrease of 0.42 m. These are significant trends. Whether these trends are indicative of the thickness trends of the Arctic Ocean is examined, as the time-varying behavior of the monthly ULS thickness distributions can be related not only to the seasonal cycle in the basal growth and melt, but also to the magnitude and pattern of ice motion in the Arctic Ocean, and the proximity of the ULS moorings to the ice edge. *INDEX TERMS:* 4207 Oceanography: General: Arctic and Antarctic oceanography; 4275 Oceanography: General: Remote sensing and electromagnetic processes (0689); 4215 Oceanography: General: Climate and interannual variability (3309); 1635 Global Change: Oceans (4203); *KEYWORDS:* Fram Strait, ice export, ice thickness

Citation: Kwok, R., G. F. Cunningham, and S. S. Pang (2004), Fram Strait sea ice outflow, *J. Geophys. Res.*, *109*, C01009, doi:10.1029/2003JC001785.

1. Introduction

[2] The sea ice outflow through Fram Strait is a major component of the mass balance of the Arctic Ocean. Roughly 10% of the total sea ice mass is exported each year through the Fram Strait. The budget presented by *Aagaard and Carmack* [1989] lists ice flux through Fram Strait as the largest single component of the Greenland-Iceland-Norwegian (GIN) Sea freshwater balance. Anomalous outflows of sea ice are significant contributors to the freshening of the surface waters of the Greenland and Labrador Seas. The strength of the global ocean thermohaline circulation is linked to these events through their impact on convective overturning of water masses [*Dickson et al.*, 1988]. Observational estimates of the ice flux at the Fram Strait are summarized by *Rothrock et al.* [2000]. The ice flux estimates, compiled over several decades (1970s through 1990s), range from 1600 to 5000 km^3/yr. Variability of the estimates over this period can be attributed to decreases in sea ice thickness, changes in large-scale atmospheric circulation associated with the Arctic Oscillation (AO) [*Thompson and Wallace*, 1998] and the North Atlantic Oscillation (NAO) [*Hurrell*, 1995], and to uncertainties in ice thickness and ice motion. The quality of ice flux estimates have improved with satellite observations, but even recent estimates by *Vinje et al.* [1998] (hereinafter referred to as VNK98) and *Kwok and Rothrock* [1999] (KR99) over the same years using the same cross-strait ice thickness profiles see differences of up to 30% using different ice motion estimates.

[3] The longer timescale connection of ice area flux to large-scale atmospheric forcing is interesting. An established link could be used as a proxy indicator of an important component of the overall Arctic Ocean sea ice mass balance and freshwater balance in the GIN Seas. KR99 reported on the co-variability of ice flux and NAO but this correlation is reduced during negative NAO years. Indeed, other investigators [*Hilmer and Jung*, 2000; *Vinje*, 2001], using model simulations and ice flux parameterizations, have also concluded that the link between ice area

0148-0227/04/2003JC001785$09.00

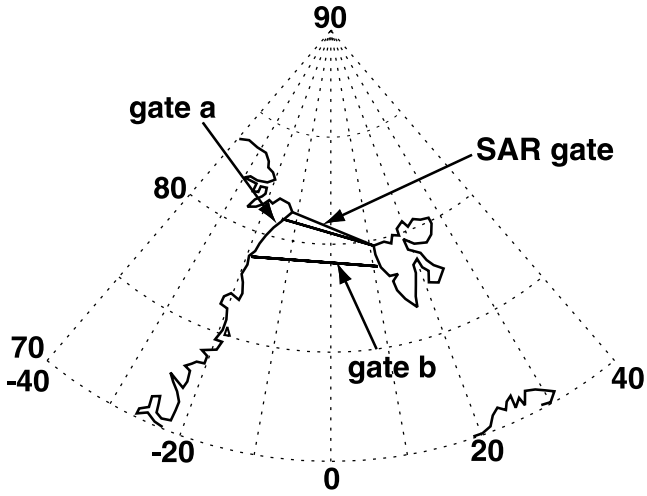

Figure 1. Location of fluxgates *a* and SAR (~81°N) and *b* (~79°N) in the Fram Strait. The volume flux is computed at *b* and the RADARSAT motion profiles (in Figure 3) are computed at SAR.

flux and the indices of the AO and NAO is more tenuous and the connection may be less robust during the negative phases of the AO and NAO. This suggests association of ice flux with a different mode of variability or a shift in the position of the common features of the North Atlantic circulation pattern that affect ice export.

[4] This work adds to that of KR99 by addressing some of the above issues and by introducing observations related to ULS observed thickness distributions. We re-examine the time series of area and volume flux, adding another 6 years of passive microwave (PMW) ice motion observations and its connection to atmospheric oscillations. Five years of high-resolution near-routine RADARSAT imagery of the Fram Strait provides another data set for more detailed evaluation and to increase our confidence in the PMW ice motion data set. Additionally, an examination of the behavior of 9 years of ULS thickness distributions shows that these observations provide revealing insights into the dynamics and thermodynamics of the Arctic Ocean sea ice cover.

[5] Section 2 provides a more thorough assessment of satellite PMW ice motion from Scanning Multichannel Microwave Radiometer (SMMR) and Special Sensor Microwave Imager (SSM/I) in the Fram Strait using buoy and Synthetic Aperture Radar (SAR)-derived displacements. The cross-strait velocity profiles from PMW ice motion are compared with those from 5 years of high-resolution ice motion. Remarkable interannual variability of the character of the Fram Strait sea ice cover can be seen in the SAR imagery. The 24 years of area flux estimates through the strait is described in section 3. The satellite-derived estimates are extended to summer using a simple parameterization of area flux. The trend in this longer time series, the link of this time series to the North Atlantic Oscillation (NAO), and the stability of this connection are reviewed. Section 4 summarizes the 8 years of volume flux estimates from ice velocity and ULS thickness estimates. The uncertainties in the volume flux estimates are discussed. Section 5 explores the 9 years of time-varying ice thickness distributions from ULS moorings in the Fram Strait in terms of their seasonal cycle, ice motion, extent of the ice stream, and the source regions in the Arctic Ocean. Anomalies in the thickness of the multiyear (MY) ice are large and seem to be dependent on the interannual variability of the above-mentioned parameters. We conclude with remarks on the observational limitations of the current approaches for estimating ice flux and the remaining uncertainties in the cross-strait thickness profiles derived from ULS moorings. The usefulness of the record of ULS thickness distributions is highlighted and the sampling issues associated with the placement of current ULS moorings are noted.

2. Fram Strait Ice Motion: PMW, SAR, and Buoy

[6] The procedure for extraction of ice motion from a region of approximately 780 km × 780 km centered around the Fram Strait fluxgates (shown in Figure 1) is detailed by KR99. Gate *a* is positioned along a ~400-km line, roughly along 81°N, drawn across the passage between Antarctic Bay in northeast Greenland and the northwestern tip of Svalbard. Fluxgate *b*, positioned farther south (~79°N), is centered in proximity of moored upward-looking sonars (ULS). We placed fluxgate *a* near 81°N since the area flux estimate across this line is more indicative of area export from the Arctic Ocean. Farther south, area is typically added by ice divergence. Daily ice motion is extracted from the 85 GHz SSM/I brightness temperature records between 1991 and 2002 and 2-day ice motion is produced from the 37 GHz records from the SMMR (1978–1987) and SSM/I (1987–2002) periods. Only winter ice motion (October through May) is available as the tracking procedure does not produce reliable estimates in the summer months.

2.1. PMW Versus Buoy Ice Motion: Comparison

[7] The positional errors in the buoy displacements (~300 m) as well as the SAR estimates (~300 m) used below are significantly smaller than the uncertainties in the PMW motion (order of kilometers) and thus are considered as truth in the following comparisons. Buoy motion is compared with the nearest 85 GHz and 37 GHz contemporaneous motion sample. The differences are shown in Table 1. For comparison, the average displacements of the samples are shown in the same table. In all cases, the mean differences between the estimates are smaller than the standard errors (noise) and the average displacements (signal). Overall, a small negative bias in the 37 GHz and a small positive bias in the 85 GHz data relative to the size of the pixels are evident. The standard error ranges between 4.4–6.4 km and 5.9–14.8 km for ice motion from the 85-GHz and 37-GHz channels. These ranges are consistent with those of *Kwok et al.* [1998]. Higher standard errors for ice motion from the lower resolution channel are expected. We note that there is a smaller number of comparisons because of the 2-day motion sampling and the smaller number of observations from the 37-GHz channel. The error statistics, especially the 37-GHz ice motion, are slightly different from that presented by KR99 as we have revised our procedure to avoid tracking sea ice within 50 km of the ice edge. This produces more reliable motion estimates.

2.2. RADARSAT Versus PMW Ice Motion

[8] Since November 1996, as part of a NASA program to monitor the Arctic Ocean ice cover [*Kwok and Cunningham*,

Table 1. Differences Between PMW Ice Motion and Buoy Motion (km)[a]

	2-Day 37V Displacements				1-Day 85V Displacements			
Year	Mean	S.D.	Number of Obs.	Mean Displacement	Mean	S.D.	Number of Obs.	Mean Displacement
1987–1988	0.9	5.9	17	18				
1988–1989	0.1	10.7	72	22.7				
1989–1990	−1.9	8.0	18	20.1				
1990–1991								
1991–1992	1.0	14.8	18	20.4	0.70	6.4	92	8.6
1992–1993	−3.3	13.8	38	21.8	0.10	4.9	217	9.2
1993–1994	−0.8	9.3	47	22.2	0.50	4.4	230	10.3
1994–1995	−1.9	11.0	49	30.2	0.00	5.7	206	14.7
1995–1996	−0.8	8.7	18	20.3	−0.30	6.0	89	12.5
1996–1997								
1997–1998	−0.1	6.2	35	15.8	1.50	4.7	182	9.3
1998–1999								
1999–2000								
2000–2001	−1.1	13.1	23	28.8	1.00	5.4	146	12.8

[a]The second, third, sixth, and seventh columns show the mean and standard deviation of the differences. The fifth and ninth columns show the mean displacement of the buoys for the observations used in the comparison.

2002], SAR coverage of the Fram Strait using RADARSAT imagery has been acquired on a routine basis. The nominal sampling interval of the region is 6 days with partial coverage varying between 1 and 12 days, depending on availability of acquisition allocations and spacecraft resources. Thus the derived displacements represent ice motion ranging from 1- to 12-day intervals. Ice motion at the SAR fluxgate (Figure 1) and its neighborhood are sampled on a 5-km grid which spans ~30 km north and south of the gate. Ice motion is derived by tracking common ice features in an image sequence using a procedure described by *Kwok et al.* [1990]. Figure 2 shows the seasonal distribution of motion observations and sampling intervals over the 5-year period, 1996 through 2001. The largest number of observations is available during the fall and winter. Ice tracking is more difficult during melt-onset in the spring because of large-scale backscatter variations associated with the appearance of liquid water on the snow layer. We have derived RADARSAT ice motion for only two summers as the reduced contrast in sea ice backscatter, important for reliable tracking, makes for an extremely difficult and time-consuming motion tracking process.

[9] As the sampling of the SAR ice motion is not uniform in time and space, the first step in the comparison is to construct equivalent PMW displacements at coincident times and locations as that of RADARSAT ice motion measurements. At a given location, the 1-day 85-GHz PMW ice motion is interpolated to provide fractional-day displacements and summed with daily estimates to obtain the net displacements with the same time separations provided by the SAR ice motion. The 2-day 37-GHz motion data set is not treated here because of the errors that would be incurred in the temporal interpolation process.

[10] The quality of the PMW ice motion is measured by the following metrics:

$$\boldsymbol{e} = \boldsymbol{u}_{PMW} - \boldsymbol{u}_{SAR}; \quad \theta = \cos^{-1}\left(\frac{\boldsymbol{u}_{PMW}\cdot\boldsymbol{u}_{SAR}}{|\boldsymbol{u}_{PMW}||\boldsymbol{u}_{SAR}|}\right);$$

$$R = \frac{\sum(\boldsymbol{u}_{PMW}-\bar{\boldsymbol{u}}_{PMW})\cdot(\boldsymbol{u}_{SAR}-\bar{\boldsymbol{u}}_{SAR})}{\sqrt{\sum(\boldsymbol{u}_{PMW}-\bar{\boldsymbol{u}}_{PMW})^2\sum(\boldsymbol{u}_{SAR}-\bar{\boldsymbol{u}}_{SAR})^2}}; scale = \frac{|\boldsymbol{u}_{PMW}|}{|\boldsymbol{u}_{SAR}|}.$$

Here $\boldsymbol{e}$ denotes the vector difference between the $\boldsymbol{u}_{\mathrm{PMW}}$ and $\boldsymbol{u}_{\mathrm{SAR}}$ motion estimates. The coordinate system is aligned with that of the SSM/I polar stereographic grid; the abscissa and ordinate are along the 45°E and 135°E meridians, respectively. The angular or directional difference between the two vectors is θ; R is the correlation between the motion vectors; and "scale" is the ratio of the displacement magnitudes of the motion estimates. Each quantity measures a different aspect of the errors in the PMW estimates.

[11] Figure 3 shows the error statistics of the 1-day 85-GHz motion data set. The correlations between the 85-GHz and SAR ice motion at the fluxgate are high (R > 0.98). The bias in e_y (the component that is near perpendicular to the gate) over the 5 years is small at ~0.4 km/day with a standard error of 6.9 km/day (Figure 3c). This result is comparable to the assessment using buoy motion presented above. We attribute the slightly higher standard error to the uncertainties introduced in the temporal interpolation

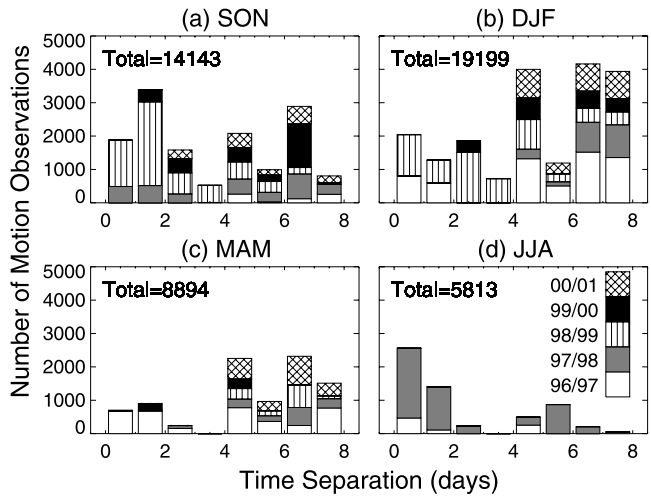

Figure 2. Histograms showing the seasonal distribution of RADARSAT ice motion observations according to their time separation and annual coverage (1996–2001). (a) September–November (SON). (b) December–February (DJF). (c) March–May (MAM). (d) June–August (JJA).

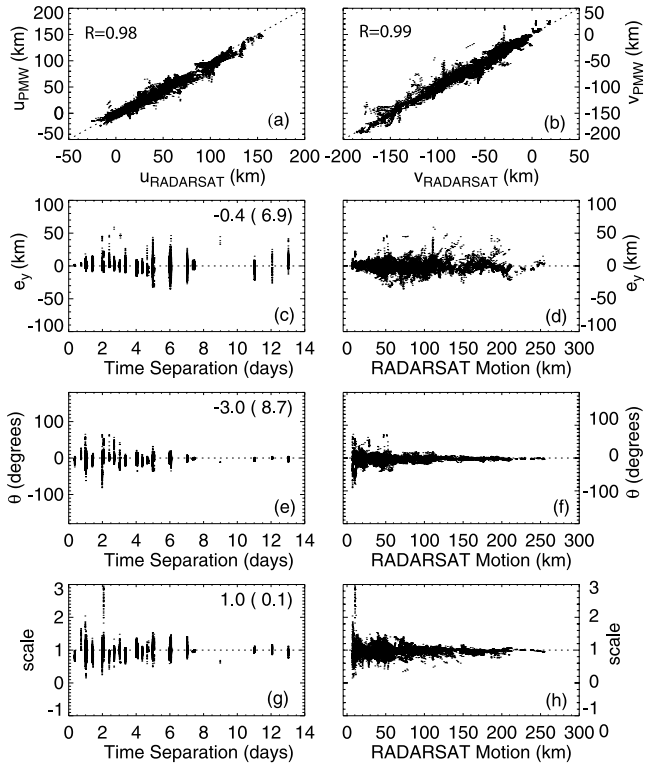

Figure 3. Comparison of 85-GHz PMW and RADARSAT ice motion. (a) Scatterplot of the x-component of ice motion. (b) Scatterplot of the y-component of ice motion. (c) Dependence of e_y on time separation, the component close to the perpendicular of the fluxgate. (d) Dependence of e_y on magnitude of motion. (e) Dependence of θ (angular difference) on time separation. (f) Dependence of θ on magnitude of motion. (g) Dependence of "scale" on time separation. (h) Dependence of "scale" on magnitude of motion. The coordinate system is aligned with that of the SSM/I polar stereographic grid where the abscissa and ordinate are along the 45°E and 135°E meridian, respectively.

process described above. The directional errors are small ($-3° \pm 8.7°$) and the scale is close to unity (Figures 3e and 3g). There does not appear to be any dependence of the motion errors on the length of time separation. When displacements and time separation are small, the standard error in θ and "scale" appear higher. This is not surprising as we expect sub-resolution scale (relative to the PMW pixels) displacements to be noisier and would give larger "scale" and directional uncertainties; that is, small displacements have lower signal content.

2.3. Cross-Strait Motion Profile

[12] The cross-strait motion profiles of KR99 are created by interpolating the gridded PMW ice motion to 20 uniformly spaced points (with ∼40 km separation) along the fluxgate. Cubic splines, constrained to go zero at the endpoints, are then fitted to the two components of the motion vectors to fill gaps in the motion estimates along the gate. SMMR and SSM/I ice concentration fields are used to mask out the ice-free samples along the line. The vectors are then projected onto the unit normal of the fluxgate to obtain the magnitude of ice motion through the passage.

[13] There are uncertainties (discussed by KR99) in using these assumptions to estimate the velocity profile in the presence of gaps in observations especially near the ice edge. Here these uncertainties are assessed using the detailed cross-strait profile from SAR ice motion. Figure 4 shows comparisons of the monthly gate-perpendicular (⊥) and gate-parallel (‖) profiles of the 85-GHz PMW and RADARSAT derived ice motion. The monthly PMW motion profiles over three periods (1991–1996, 1996–2002, and 1991–2002), except for November, are very similar. We note that the November gate-perpendicular motion between 1996 and 2002 is higher than 1991–1996. The RADARSAT profiles, from SAR observations between 1996 and 2001, are sampled at a higher spatial density (approximately every 5 km). Because of temporal gaps in the SAR motion record, the profiles may not properly reflect the monthly mean. The broad agreements in the cross-strait profiles in magnitude and shape indicate that the boundary condition assumptions are reasonable. There is a slight mismatch at the western boundary of the gate; the RADARSAT profiles go to zero faster than that of the PMW profiles since the western endpoint of the PMW gate (gate *a*) is positioned somewhat farther west than the SAR fluxgate (Figure 1). In any case, the sharp motion gradient near the Greenland coast is smoothed by the lower resolution PMW observations. The June and September profiles show the slowest motion overall. No PMW ice motion is available during July and August. The gate-parallel motions are smaller in magnitude (∼2–3 km/day versus ∼10–20 km/day near the center of the strait) and consequently have higher relative uncertainties.

[14] It is also interesting to examine the RADARSAT imagery over the Fram Strait. The spatial resolution of the SAR imagery (∼100 m) shows a wealth of detail of the sea ice characteristics in Fram Strait and that portion of the ice cover sampled by upward-looking sonar moorings placed near the shelf break. Figure 5 shows RADARSAT imagery of the ice cover during early, middle, and late winter over 4 years and the corresponding location of the ULS moorings. As the Arctic Ocean sea ice rounds the western most tip of Greenland (Nordostrundingen), it carries with it radiating fracture patterns that were formed upstream and locally. Lower backscatter first-year ice exported from the Northeast water polynya, south of Nordostrundingen, is evident in all the images. This first-year ice covers the largest area in the winter of 1998/1999. Variability in the width of the ice stream and the size of ice floes can be seen in the sequences of winter images. High backscatter wind-roughened open water is seen to the east of the ice stream. This bright open water backscatter signature is not evident within the ice stream, suggesting little open water and high ice concentration inside the ice edge. During late fall and early winter, the ice stream appears more consolidated with a dominant fraction of large and distinct multiyear (MY) ice floes. Near the end of winter, the ice cover consists of smaller MY floes probably due to convergence/fracturing of a more consolidated and thicker Arctic Ocean ice cover upstream of the strait and the divergence of the ice cover downstream of the Fram Strait. Of the 4 years, the width of the ice stream is narrowest and the FY-ice fraction is highest during the winter

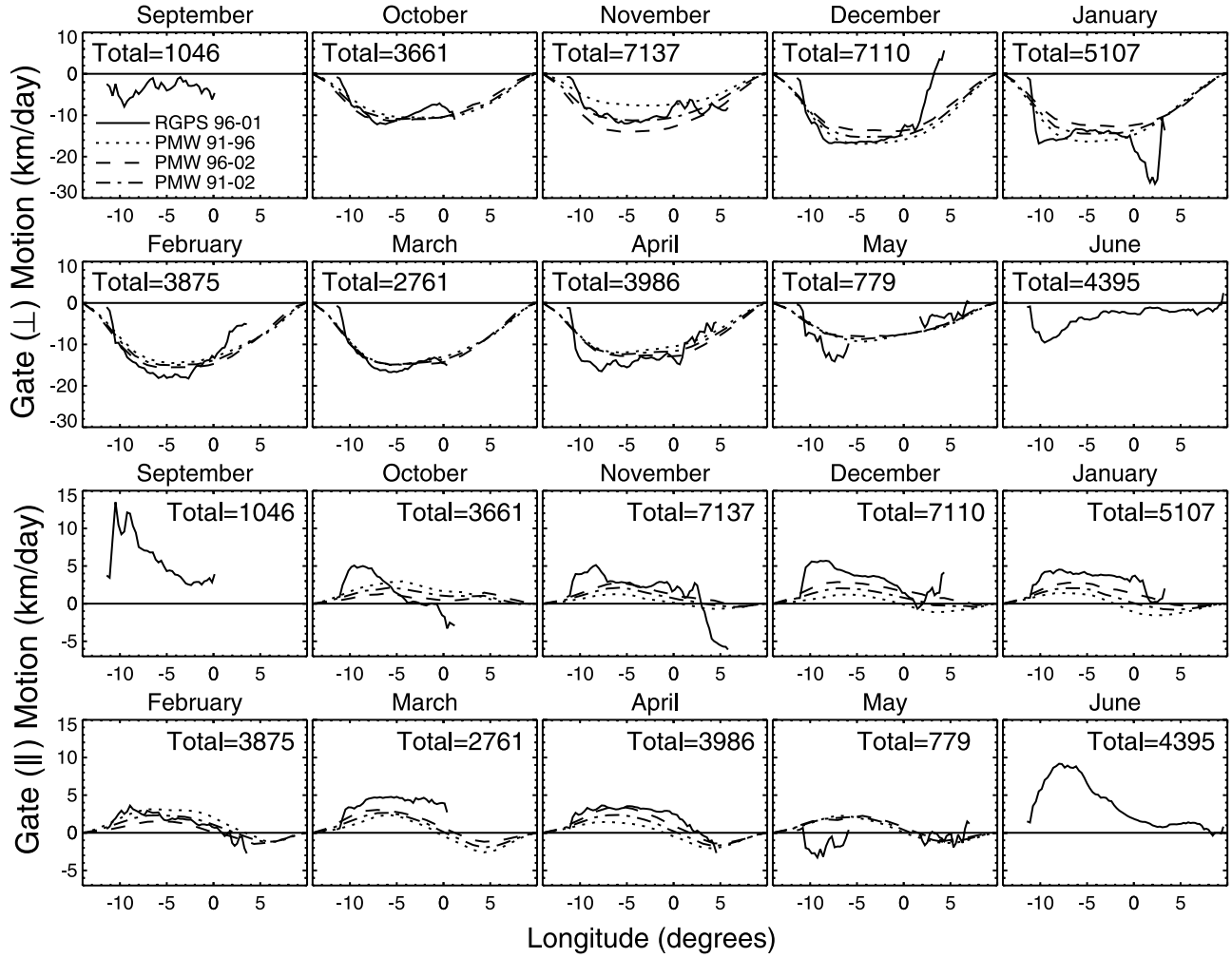

Figure 4. Comparison of monthly gate perpendicular (⊥) and parallel (||) motion profiles from 85-GHz PMW and RADARSAT ice motion. The key for the line styles is shown in the top left plot. The solid lines show the RADARSAT motion profiles while the different styles of dashed lines show the average monthly PMW motion profiles over the years 1991–1996, 1996–2002, and 1991–2002.

of 1998/1999. Discussed in section 5, these anomalies in the distribution of ice types are reflected in the ice thickness distribution constructed from ULS observations.

3. Area Flux (1978–2002): 24 Years

[15] The area flux, F, is estimated by summing the ice flux over the 19 segments along the fluxgate using the simple trapezoidal rule, $F = \sum_1^{19} 0.5(u_i + u_{i+1})\Delta x$, where u is the magnitude of the motion perpendicular to the fluxgate and Δx is the spacing between the motion estimates.

3.1. Area Flux Estimates From PMW Ice Motion

[16] The 85-GHz and 37-GHz winter area flux are the total of the daily and 2-day area flux from the beginning of October until the end of May. Figure 6 and Table 2 summarize the winter area flux at gate a for the 8 years (1991–2002) of 1-day 85-GHz motion observations and the 24 years (1978–2002) of 2-day 37-GHz ice flux estimates. Compared to KR99, the construction of the 37-GHz cross-strait profiles here includes an additional filtering step. Because of the frequency of outliers associated with the variability of the brightness temperature fields near the ice edge, the motion estimates within 50 km of the ice edge are discarded. This filter increases the 37-GHz area flux by an average of ~30,000 km^2 and reduces the difference between the 37-GHz and 85-GHz flux estimates. The trend and the value of the ice flux from the two records are now quite consistent over the 8 years with overlapping observations (Figure 6a). The average area flux over this period is 803,000 km^2 with a standard deviation of 97,000 km^2. The mean difference between the two winter flux estimates is ~−12,000 km^2 with a standard deviation of 50,000 km^2 (see Figure 6a).

[17] The average winter (October–May) area sea ice flux over the 24-year record (1978–2002) of ~754,000 km^2 can be compared to average winter area flux estimate of 670,000 km^2 over the 18-year record (1978–1996) of KR99. The winter area flux ranges from a minimum of 607,000 km^2 in 1990/1991 to a maximum of 952,000 km^2 in 1994/1995. The standard deviation in the annual winter flux is 86,000 km^2. Over the longer record, there is an

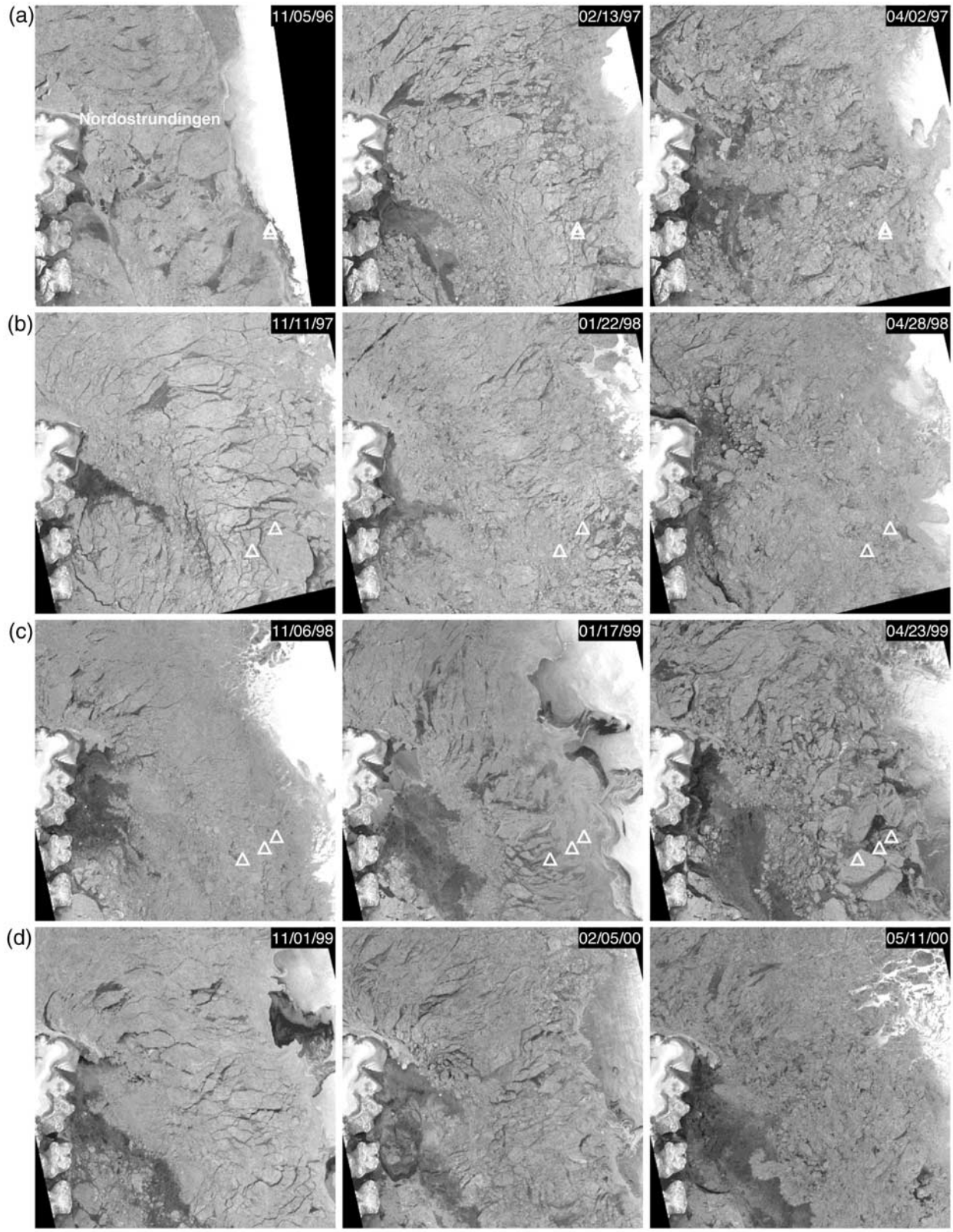

Figure 5. RADARSAT imagery of the Fram Strait sea ice in early, middle, and late winter over 4 years. (a) 1996/1997. (b) 1997/1998. (c) 1998/1999. (d) 1999/2000. The bright saturated radar returns are from wind-roughened open water. The location of the eastern tip of Greenland, Nordostrundingen, is shown on the top left panel. (RADARSAT imagery © CSA 2002). Triangles mark the locations of upward-looking sonar moorings.

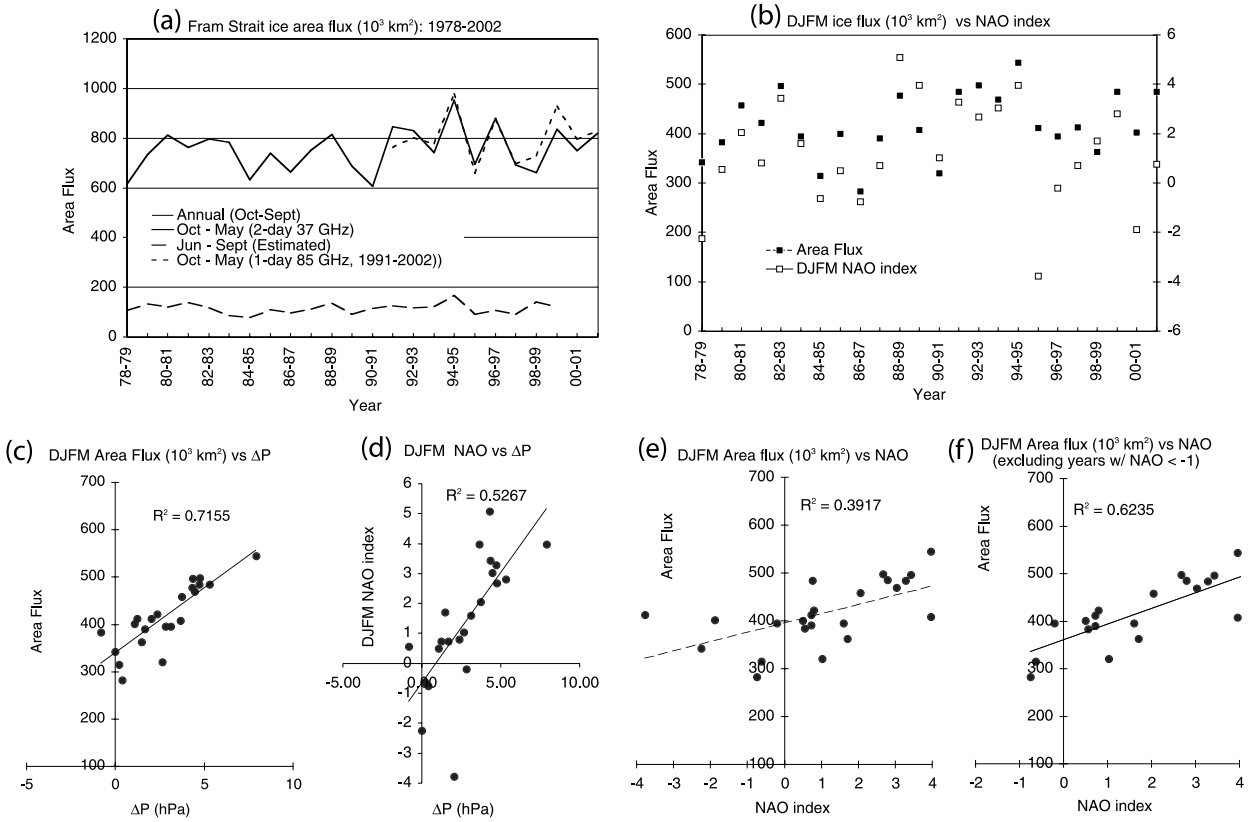

Figure 6. Fram Strait ice area flux (1978–2002). (a) October through May, June through September, annual, and 85-GHz October through May area flux. (b) DJFM area flux and DJFM NAO index. (c) DJFM area flux as a function of cross-strait atmospheric pressure gradient (ΔP). (d) DJFM NAO index as a function of cross-strait atmospheric pressure gradient (ΔP). (e) DJFM area flux as a function of DJFM NAO index. (f) DJFM area flux and DJFM NAO indices >−1.

Table 2. Fram Strait Sea Ice Area Flux at Gate *a* (10^3 km^2)

	2-Day 37-GHz Ice Motion										
Year	Oct.	Nov.	Dec.	Jan.	Feb.	March	April	May	Oct–May	June–Sept[a]	Annual
1978–1979	27	82	76	91	75	99	68	94	614	108	722
1979–1980	87	148	117	94	82	90	84	32	735	133	868
1980–1981	103	87	140	132	95	90	99	67	813	119	933
1981–1982	86	101	108	99	112	104	106	47	763	137	900
1982–1983	39	107	132	154	99	110	106	48	796	118	914
1983–1984	107	107	114	57	135	89	101	72	782	86	868
1984–1985	55	75	47	93	75	99	116	71	631	79	710
1985–1986	99	93	133	85	83	98	67	82	740	109	849
1986–1987	128	115	47	38	118	79	82	55	663	95	758
1987–1988	82	98	103	102	63	121	119	63	753	112	865
1988–1989	55	116	103	136	104	135	113	53	814	136	949
1989–1990	89	72	105	75	119	108	61	58	688	92	780
1990–1991	90	76	126	88	46	60	71	49	607	113	720
1991–1992	93	94	125	118	110	131	85	91	847	124	970
1992–1993	72	77	128	140	129	101	95	89	830	117	947
1993–1994	80	24	110	137	74	148	118	49	741	123	864
1994–1995	151	103	135	137	147	126	132	22	952	166	1119
1995–1996	60	58	109	94	91	117	92	72	694	92	786
1996–1997	125	160	92	119	79	105	127	73	879	108	986
1997–1998	119	65	85	107	92	128	23	74	693	91	784
1998–1999	94	100	92	87	76	108	91	14	661	139	800
1999–2000	78	99	124	134	109	117	103	71	836	122	958
2000–2001	78	101	119	66	123	93	107	61	749		
2001–2002	55	119	104	96	158	127	100	62	821		
Avg.	86	95	107	103	100	108	94	61	754	115	866
S. D.	28	27	24	28	27	19	24	20	86	20	101

[a]Estimated from cross-strait pressure gradient and May ice flux profile.

upward trend in the ice flux of approximately 3040 km^2/yr, smaller than the 9900 km^2/yr given by KR99. The larger trend in the shorter 18-year time series is likely a result of the bias introduced by the large flux year of 1994/1995 at the tail of the series.

[18] The correlation between the DJFM sea ice area flux and cross-strait pressure gradient remains high at 0.85 (Figure 6c). Following KR99, we estimate the monthly summer area flux, F_{summer}, shown in Table 2 using the following updated relationship (22 years),

$$F_{summer} = 5827\Delta P + 78726 \ (\mathrm{km}^2),$$

where ΔP (mbar) is the mean monthly pressure gradient across the Fram Strait. The residual of the regression analysis is 3400 km^2/yr or 12% of the average monthly area flux. It is important to note that this approach does not take into account the following season-dependent factors that might affect the area flux estimates: reduced internal ice stress during the summer; varying stability of the lower atmosphere affecting air/ice momentum exchange; and variability in the summer ice concentration. The time series of ice flux during the summer months is shown in Figure 6a. Including the summer area flux, the average annual ice area flux is 866,000 km^2/yr over the 22-year record. The summer months contribute approximately 15% of the ice area to the annual area exported through the Fram Strait. Between the 1980s and 1990s, the decadal difference in the net exported ice area is $\sim$400,000 km^2, approximately half the annual average.

3.2. NAO, Ice Area Flux, and Cross-Strait Pressure Gradient

[19] Because of the dominance of the NAO versus AO in the Atlantic-Arctic sector and their similarities in the winter, we focus on ice flux and the NAO record. Over the 24-year record, the NAO index explains $\sim$39% of the variance in the DJFM ice area export and $\sim$53% of the variance in the DJFM cross-strait pressure gradient (Figures 6d and 6e). During the positive phases of NAO, the pressure contours are positioned in such a manner as to increase the SLP gradient across the Fram Strait, and thus the strengthening of the meridional winds driving ice export. KR99 also noted that the correlation between the area flux and NAO index is reduced during the negative phases of the NAO index; the longer record here reinforces this observation. This is especially evident in Figure 6b where the decreases in ice area flux do not follow the negative extremes in the NAO index. As the winter NAO indices are in a negative phase prior to 1978, this may be indicative of reduced correlations during periods when the indices are of negative polarity. Excluding the three winters (1978/1979, 1995/1996, and 2000/2001) with extreme negative indices (NAO < -1), the NAO index explains $\sim$62% of the variance in the DJFM ice area export (Figure 6f). Similarly, the scatterplot (Figure 6d) of the DJFM NAO index versus the cross-strait pressure gradient shows higher scatter of the points at negative extremes of the NAO indices.

[20] The connection of ice area flux to large scale atmospheric forcing at longer timescales, beyond the satellite era, is interesting. An established link could be used as a proxy indicator of ice export, an important component of the overall Arctic Ocean sea ice mass balance. The variability of this component has significant climatic consequences. In a model simulation, *Hilmer and Jung* [2000] noted that the increased coherency between NAO index and ice area flux from 1978 through 1997 is associated with an eastward shift of the centers of action of this atmospheric oscillation. Prior to this period (1958–1978), they find negligible correlations between the NAO and ice area flux time series. A recent study by *Vinje* [2001] also found that the observed positive correlation between the period 1978–2000 is not representative of the character of the two time series when a longer period (1950–2000) is examined. More recently, *Cavalieri* [2002] reported on a link between the January Fram Strait ice flux and the phase of the zonal wave-1 sea level pressure. Excluding the years 1966 and 1967, his analyses suggest this zonal wave-1 phase explains 60–70% of the simulated ice export from two different models for the 40-year period between 1958 and 1997. It is not clear, however, how robust this connection is when extended to other winter months. The physical mechanisms associated with the atmospheric variability indicated here are complex and beyond the scope of this discussion. However, the identified relationships are useful as diagnostic tools for climate models and for the eventual understanding of the underlying mechanisms of these associations.

4. Volume Flux (1991–1998): 8 Years

[21] The volume flux is computed at gate *b* rather than gate *a*, in the neighborhood of where most of the thickness data from ULS moorings are located.

4.1. Ice Thickness: Upward-Looking Sonar Data

[22] To maintain consistency with KR99 in the volume calculations, we use the parameterization of the monthly cross-strait ice thickness profile, h, (a function of longitude, λ) of VNK98, namely,

$$h(\lambda,t) = \begin{cases} h_o(t)(-0.127\lambda + 0.37) & 0^\circ < \lambda < 2.9^\circ \\ 0.68h_o(t) & -5^\circ < \lambda < 0^\circ \\ h_o(t) & \lambda \le -5^\circ, \end{cases}$$

where $h_o(t)$ is the thickness at 5°W. This thickness profile is derived from upward-looking sonar (ULS) observations at different locations and times in 1992, 1993, and 1995. The monthly mean h_o, between October 1990 and July 1996 from ULS measurements are given in Table 7 of VNK98. To maintain consistency, the same procedure described by VNK98 is used to reduce the ULS observations at different longitudes to estimate $h_o(t)$ for the years 1996 through 2000. An expected uncertainty of 0.1 m is reported for individual ULS estimates, but we believe that there is considerable uncertainty in the assumed cross-strait thickness profile due to sampling and data available for its derivation. Thus it may not be representative of the profiles in other years. Also, discussed in the next section, this profile may be dependent on the magnitude and pattern of ice motion in the Arctic Ocean as well as proximity of the ULS moorings to the ice edge.

4.2. Volume Flux Estimates

[23] With the cross-strait thickness profile, $h(x,t)$, described above, the monthly winter volume flux is calculated as

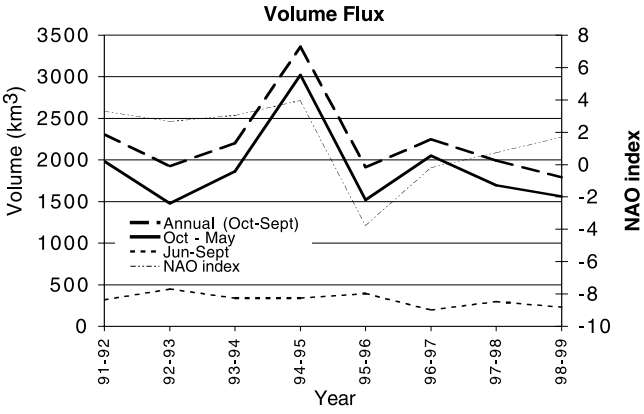

Figure 7. Volume flux at gate *b*.

$F_v(t) = \int_{coast}^{iceedge} h(x,t)u(x,t)dx$, where x is the distance along the fluxgate and $u(x, t)$ is the motion profile at 79°N (gate *b* in Figure 1). A set of motion profiles along this gate, different from that used in the area flux calculations, is derived from the gridded PMW ice motion fields using the procedures described in section 2. Here the monthly ice volume flux is taken as the sum of the product of the monthly mean ice velocity and the monthly mean ice thickness across this fluxgate. In general, we note that this may be different from the monthly sum of more frequently sampled (say, daily) volume flux; implicit in this assumption is that the covariance between the velocity and thickness time series is small.

[24] Summer volume flux is estimated by first estimating the monthly velocity profiles at gate *b*. Since we do not have motion measurements during the summer, this is accomplished by using the summer area flux (estimated using the procedure discussed in section 3) to weigh an area-normalized May motion profile, $\tilde{u}$(x), across gate *b* to obtain an estimated motion profile, $u(x, t) = A_{summer}(\Delta P,t)\tilde{u}(x, t)$ [KR99]. The volume flux, F_V, is then computed using the thickness data as described above.

[25] Figure 7 and Table 3 show the total, winter, and summer ice volume flux estimates. The mean annual volume flux over the period 1991–1998 is 2218 km^3/yr (~0.07 Sv), compared to a 5-year mean of 2366 km^3/yr (0.075 Sv) of KR99. The volume flux ranges from a minimum of 1914 km^3/yr(~0.06 Sv) in 1995/1996 to a maximum of 3363 km^3/yr (~0.11 Sv) in 1994/1995. The DJFM volume flux accounts for ~50% of the annual ice volume flux. The interannual variability in the annual winter flux is high with a standard deviation of 497 km^3 (0.015 Sv), and there is no significant trend over the record. The NAO index explains ~43% of the variance in the 8-year DJFM volume flux record.

[26] A fairly extensive review of the published observational estimates of volume flux at Fram Strait is given by *Rothrock et al.* [2000]. In the same volume, *Lewis* [2000] highlighted the differences between the contemporaneous ice export estimates of VNK98 and KR99; the VNK98 estimates are higher, in 1 year over 30%, than that given by KR99. To examine the differences, we discuss the differences between the two approaches to estimate ice flux. Since the two procedures use identical cross-strait ice thickness parameterization, the only differences are (1) VNK98 ice motion is derived from the cross-strait sea level pressure gradient, while the KR99 ice motion is derived from satellite passive microwave data and (2) the assumed cross-strait velocity profiles. First, there is uncertainty in ice motion derived from pressure gradients. Second, VNK98 use an exponential ($e^{0.08L}$, L = −12.5, −7.5 and −2.5) to describe the shape of the increasing velocity profile in three intervals between 15°W and 10°W, 10°Wand 5°W, and 5°W and 0°. The SAR profiles in Figure 4 show quite clearly that the exponential profile is not representative of the actual motion profile. Additionally, this exponential profile is non-zero at the coast of Greenland and thus contributes significant volume to the total flux. We are therefore not surprised at the larger flux estimates obtained by VNK98. We believe that the largest source of the discrepancy in the volume flux estimates of VNK98 and KR99 is due to the differences discussed here. Our assessment of the quality of our motion data set shows the PMW motion estimates to be relatively unbiased when compared with buoy and SAR ice motion. The comparative analysis of the PMW (passive microwave) ice motion and 5 years of synthetic aperture radar (SAR) ice motion shows that the uncertainty in the estimates to be consistent with that given by KR99, giving greater confidence in our record of ice flux calculations.

5. Time-Varying Ice Thickness Distribution From ULS

[27] The time-varying monthly ice thickness distribution sampled by ULS moorings in the Fram Strait is interesting. As we use these thicknesses for estimating volume flux, the associated question is whether these estimates are good

Table 3. Fram Strait Sea Ice Volume Flux at Gate *b* (km^3)

	2-Day 37-GHz Ice Motion									
Year	Oct.	Nov.	Dec.	Jan.	Feb.	March	April	May	June–Sept.[a]	Annual
1991–1992	248	248	265	253	256	342	153	222	319	2306
1992–1993	135	140	209	207	196	284	162	143	450	1926
1993–1994	144	−2	338	346	146	437	338	116	339	2202
1994–1995	359	289	509	379	347	482	475	186	339	3364
1995–1996	152	121	176	215	164	244	251	197	395	1915
1996–1997	233	250	183	261	254	290	398	182	195	2248
1997–1998	227	142	198	242	230	327	67	261	297	1992
1998–1999	162	246	267	190	253	197	172	73	232	1792
Avg.	208	179	268	262	231	325	252	173	321	2218
S. D.	76	97	112	67	63	95	140	60	82	497

[a]Uses area flux estimated in Table 2.

indicators of the ice thickness in the Arctic Ocean and whether local processes and advection affect these observations. Figure 8 shows composites of the time-ice thickness distribution diagram over the 9 years of ULS observations constructed using the eleven individual moorings shown in Table 4. The locations of these moorings, for the years with SAR data coverage, are shown on the imagery in Figure 5. The Norwegian Polar Institute provides these monthly ice thickness distributions. As the availability and location of ULS moorings change from year-to-year, only the ones located in the neighborhood of fluxgate *b* (i.e., within 0.5° of 79°N) are used here. This limits the meridional variability seen in the distributions. Figure 8c shows the composite of the thickness distributions of the ULS moorings west (Figure 8a) and east (Figure 8b) of 4.6°W. The intent of this separation is to show potential cross-strait variability seen by the ULS. Overlapping distributions are averaged to form the composite shown in Figure 8c. This composite is then separated into their winter (Figure 8d) and summer (Figure 8e) components to highlight the seasonal character and anomalies in the time-varying ice thickness distributions.

[28] Another data set that is useful for understanding the observed ULS thickness distributions is the variability of the width of the ice stream provided by the passive microwave ice concentration estimates. The proximity of the ULS moorings to the ice edge, and therefore to the warmer open ocean where melt occurs, is provided by the variability of this width. Figure 9 shows the 24-year record of mean seasonal ice concentration and its anomalies along fluxgate *a*. Using the 30% ice concentration isopleth to define the edge of the ice stream, the mean width varies between 394 ± 39 km for DJF, 401 ± 29 km for MAM, 384 ± 32 km for JJA, and 354 ± 41 km for SON. The widest is found in mid-winter (MAM) while the narrowest in late-summer and fall (SON), an average difference of 50 km between the two seasons. Over the ULS record, the most prominent negative anomaly, or the narrowest winter width (∼300 km in DJF) can be found during the winter (DJF and MAM) of 1998/1999. The winter of 1994/1995 has the widest ice stream (>400 km).

5.1. Seasonal Cycle

[29] We first discuss the general features before we examine the anomalies seen in the composite (Figure 8). The winter distributions with typical modal peaks at ∼3 m and at ∼0.5–1.0 m provide an effective distinction between the multiyear (MY) and first-year (FY) ice classes. The color scale represents the magnitude of the population density (red: high, blue: low). The increases and decreases in thickness of the multiyear ice modes over the winter and summer, perhaps largely due to growth and melt, are the most striking features of the seasonal cycle in the composite. The increases in thickness of the MY mode over the 8 months of winter (November–April) range between ∼0 m to 1.4 m (average: 0.75 ± 0.53 m) and the decreases over the summer (June–September) range between ∼0.1 m and 1.0 m (average: −0.5 ± 0.32 m). Zero growth is assumed for the transition months of May and October. These rates are obtained by regression of the thickness of the MY modes against time between the winter (November–April) and summer endpoints (June–September). The interannual variability is high. The winter trend is comparable but seems higher than could be explained by thermodynamics alone, if the typical basal growth of a 3-m floe is ∼0.5 m [*Steele and Flato*, 2000], although the variability of this quantity is not well known. Since the moorings do not provide a Lagrangian view of the ice cover, processes other than growth and melt contribute to the observed variability in the thickness distribution. In winter, ice deformation could contribute to increases in thickness of the MY modes (in the 3-m range) as ridging and rafting creates thicker ice, but it is not clear that this would alter the thickness mode significantly. An additional trend in the MY mode could be attributed to the time-dependent trend of export of thicker or thinner ice from the interior of the Arctic. Whether these factors are significant contributors to the winter trend is a question. The mean summer melt (top and bottom) of 0.5 m is comparable to that of *Steele and Flato* [2000]. Variability of the summer ice trend could also be attributed to the increased proximity of the moorings to the ice edge causing increased melt as it retreats over the season. In this time sequence, we note here that there are two anomalous winters (1992/1993 and 1998/1999, discussed below) where the winter trend in thickness is close to zero.

[30] The behavior of the FY mode is not particularly remarkable relative to the MY mode during the winter or summer. The thickness of seasonal FY ice depends on where and when this ice is created and its seasonal age and thickness would thus show a larger variability and present less of a coherent trend in the ULS observations. The mean of the distribution (dashed line in Figure 8c), as expected, is highly correlated to the thickness of the MY mode. The higher variability of the mean could be attributed to the variability in open water fraction in the thickness distribution.

5.2. Ice Motion and Source Regions

[31] In addition to the thermodynamic record that is present in the time history, the MY mode could provide an indication of the thickness distribution of the source regions of the ice thickness sampled at these moorings. To explore this connection, we plot the source location of the ice crossing the fluxgate over the nine winters (1991–1999) associated with

Figure 8. Nine years (1991–1999) of time-dependent ice thickness distribution (>10 cm) from upward-looking sonar (ULS) data from the Norwegian Polar Institute. Only ULS data between 78.4°N and 79.3°N are shown here. (a) ULS measurements west of 4.6°W. (b) ULS measurements east of 4.6°W. (c) Average over all ULS measurements. Solid and dashed lines connect the monthly mode of the multiyear and mean ice thicknesses, respectively. There is an overall decrease of 0.45 m in the mean ice thickness over the entire time series and a decrease of 0.23 m during the winter months (DJFM). Similarly, the mode of the MY ice exhibits a decrease of 0.55 m over the entire time series and a decrease of 0.42 m during the winter. (d) Winter (Oct–May). (e) Summer (May–Oct). Colors (from blue to red) denote the relative density of the thickness category. Slopes of the multiyear ice modes are shown in Figures 8d and 8e.

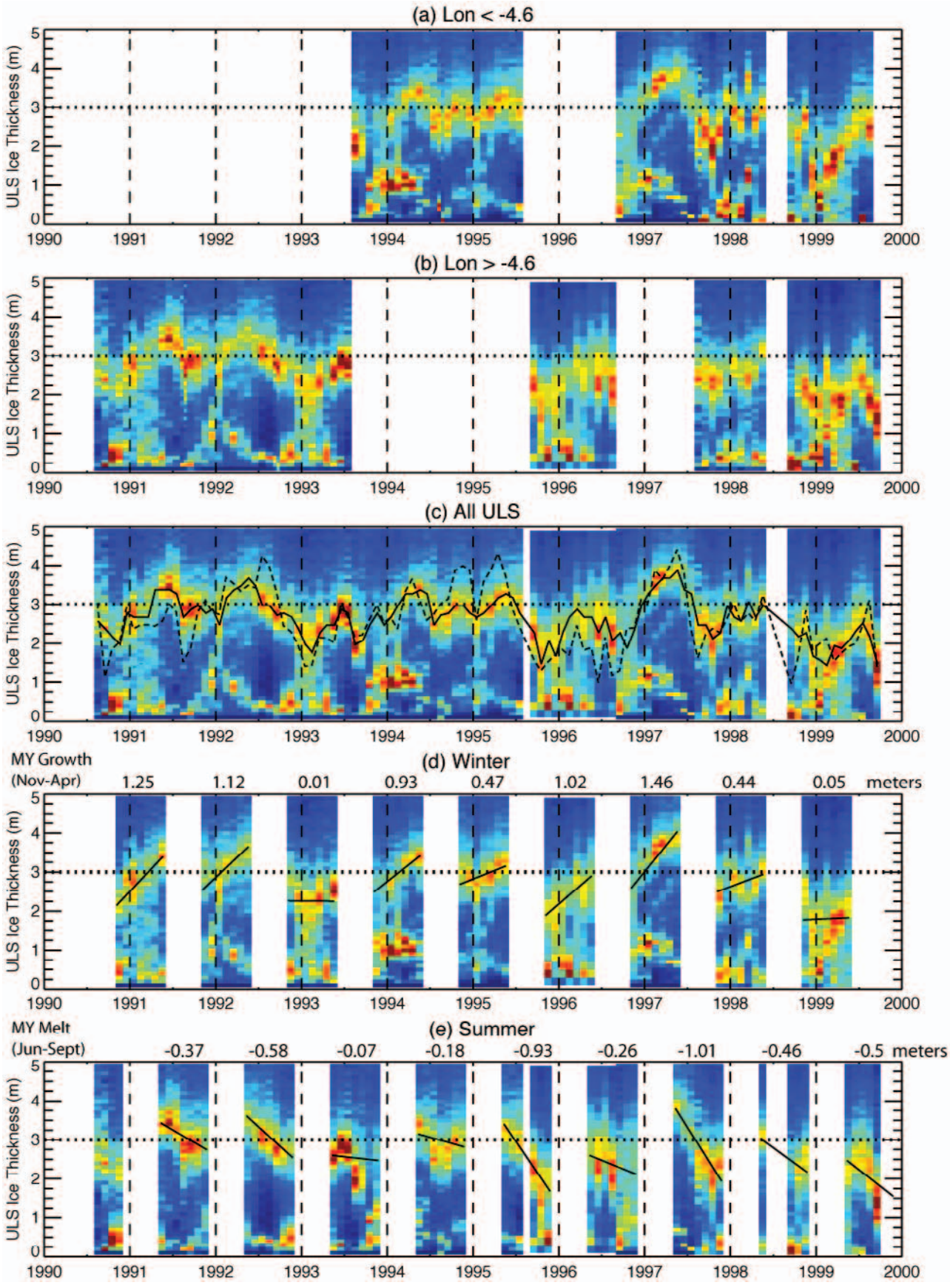
(a) Lon < -4.6
(b) Lon > -4.6
(c) All ULS
(d) Winter
MY Growth
(Nov-Apr)
1.25 1.12 0.01 0.93 0.47 1.02 1.46 0.44 0.05 meters
(e) Summer
MY Melt
(Jun-Sept)
-0.37 -0.58 -0.07 -0.18 -0.93 -0.26 -1.01 -0.46 -0.5 meters
ULS Ice Thickness (m)
0 1 2 3 4 5
1990 1991 1992 1993 1994 1995 1996 1997 1998 1999 2000

Table 4. Upward-Looking Sonar Data Used in This Paper

Latitude	Longitude	Start, dd/mm/yy	End, dd/mm/yy	ULS ID
79.22°N	3.38°W	08/08/90	20/08/91	sn03
79.08°N	3.73°W	21/08/91	09/10/92	sn03
78.45°N	4.40°W	27/08/92	07/09/93	sn12
79.00°N	6.01°W	28/07/93	08/07/94	sn16
79.00°N	7.03°W	07/08/94	21/07/95	sn12
78.07°N	4.44°W	01/09/95	09/06/96	sn17
78.93°N	5.00°W	05/09/96	30/08/97	sn32
78.97°N	6.32°W	27/08/97	09/04/98	sn17
79.00°N	4.28°W	27/08/97	30/05/98	sn44
79.03°N	6.85°W	09/09/98	21/09/99	sn34
78.98°N	4.26°W	11/09/98	19/09/99	sn37

ULS observations. Figure 10 shows the November location of the ice crossing fluxgate *a* for the months of December through May. These are created by back propagation of the 1-day 85-GHz PMW ice motion fields of the Arctic Ocean. The regional contribution of the ice exported for a particular year can be seen in the penetration of the central Arctic by the isochrones, the preferences of these contours for the central, eastern, and western Arctic ice cover, and the width of coverage of these contours. In the winter with the largest ice export (1994/1995) and a high NAO index (close to 4), sea ice close to the North Pole can actually be seen at the Fram Strait. The mean thickness of the MY ice mode is ~3 m. Similarly, the winter (1996/1997) with the thickest MY ice mode (~3.5 m) and also having a source region close to the Pole suggest this to be a good proxy indicator of the regional thickness within the Arctic.

[32] In contrast, the thinnest MY ice mode of ~1–2 m is found during the winter of 1998/1999. This is the winter where the axis connecting the points of these isochrones (defined by the midpoint at the gate) shows an extreme inclination toward the east, closer to the summer ice edge, where thinner MY and FY ice are typically found. We attribute the observed ULS thickness to be characteristic of this source region in the Eastern Arctic. Examining the SAR images of this winter (Figure 5c) shows the ice cover to be different, with fewer well-defined MY floes, and to be less compact especially at the end of the winter. This is also the summer with the narrowest ice stream over the ULS record. We suspect that more FY ice from the Eastern Arctic is entrained into the ice stream before it is exported through the Strait. During the winter of 1993/1994, a bimodal thickness distribution with a significant FY mode at ~1 m is evident. Here the axis also shows an eastern inclination and preference for ice from the Eastern Arctic. Again, we believe this to be indicative of the ice thickness of the source region as a result of ice motion.

[33] We also expect the observed ice thickness to be dependent on the location of the perennial ice edge during the winter. If that edge is displaced toward the west, and if the atmospheric circulation and ice motion favor source regions in eastern Arctic Ocean, then one can expect thinner FY ice to be the dominant peak in the thickness distribution. Similar to the discussion above, there is no pronounced trend in the FY mode due to the large variability expected in this seasonal ice.

5.3. Interannual Variability

[34] The above discussion focuses on the broad features seen in the time-ice thickness distribution diagrams. No direct connection between the thickness distributions and

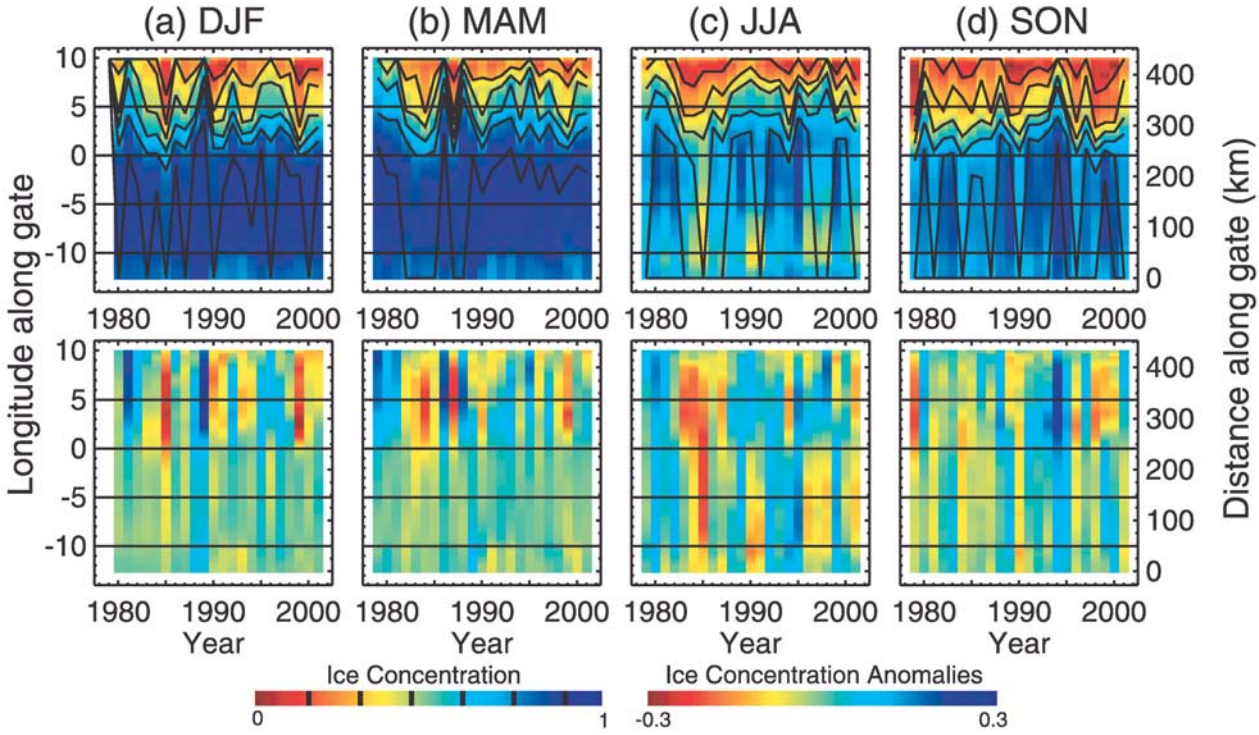

Figure 9. Seasonal passive microwave ice concentration and ice concentration anomalies (1978–2002) along fluxgate *a*. (a) December–February (DJF). (b) March–May (MAM). (c) June–August (JJA). (d) September–November (SON).

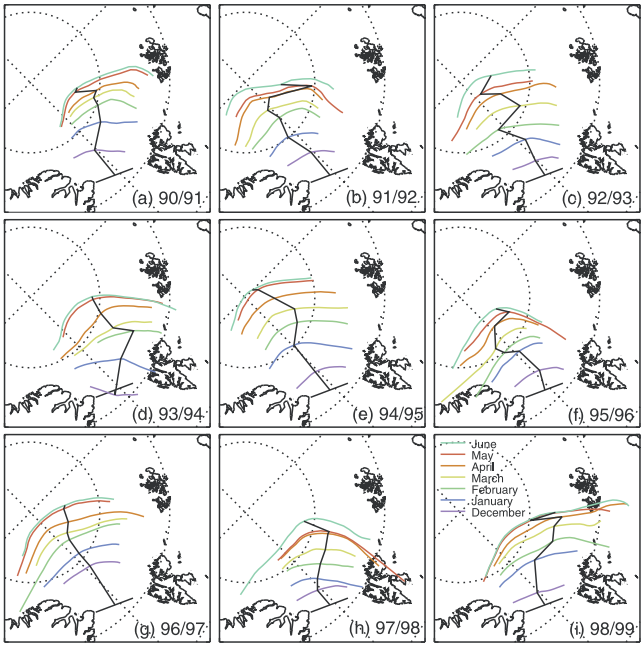

Figure 10. November location of the ice crossing fluxgate *a* in December, January, February, March, April, and May. (a) 1990/1991. (b) 1991/1992. (c) 1992/1993. (d) 1993/1994. (e) 1994/1995. (f) 1995/1996. (g) 1996/1997. (h) 1997/1998. (i) 1998/1999. The trajectories are derived from passive microwave ice motion.

the AO or NAO is seen. Because ice thickness is an integrator of the surface mass and energy balance of the Arctic Ocean, the interactions may be more complex and connections may not be apparent. The expression and magnitude of the seasonal cycles ultimately depend on the history of atmosphere and ocean conditions in the Fram Strait and within the Arctic Ocean. For example, the smaller winter growth rates in 1992/1993 and 1994/1995 have minimums in thickness later in the season (in January). Similarly, the summer minimum thickness appeared earlier during the summer of 1994 (in July). These misplaced extremes bias the regression estimates. On a seasonal to annual timescale, could the smaller increase in MY ice thickness during the winter of 1994/1995 and the large decrease in thickness during the 1995 summer be associated with the retreat of the cold halocline layer (CHL) described by *Steele and Boyd* [1998]? The absence of this insulating layer (from the warm Atlantic layer below) would reduce winter ice growth upstream of the ULS moorings and changes in ice thickness, as suggested by *Martinson and Steele* [2001], may perhaps be the only reasonable diagnostic of the activation of the ocean heat flux. Recent partial recovery in the CHL has been reported by *Boyd et al.* [2002] and *Björk et al.* [2002]. This potential link is compelling but a longer-term continuous time series description of the cold halocline layer of the Arctic Ocean to establish this connection is not yet available. Locally, the effect of the NAO-related warming of the warmer and more saline West Spitsbergen Current [*Dickson et al.*, 2000] on Fram Strait ice thickness remains to be analyzed.

[35] Over the ~9-year period shown here, we computed the trend in the ice thickness of the mean and the mode of the thickness distribution of the entire time series and for the winter months of December through March. There is an overall decrease of 0.45 m in the mean ice thickness over the entire time series and a decrease of 0.23 m during the winter. Likewise, the mode of the MY ice exhibits a decrease of 0.55 m over the entire time series and a winter decrease of 0.42 m. These are significant trends. Whether these decreases in thickness is a reasonable diagnostic of trends in the mean ice thickness within the Arctic Ocean is subject to all the caveats discussed above. Namely, the source regions of the sea ice, the proximity of ULS mooring to the ice edge, and perhaps the deformation of the ice cover. The significant interannual variability of the seasonal cycles in the thickness distributions suggests this signal to be a potentially good indicator of ice/ocean/atmosphere interactions locally and upstream in the Arctic Ocean. There is much about the data, especially the interannual variability, that is left unexplained. Although beyond the scope of this paper, we believe that the observed anomalies in these records provide clues to the behavior of the Arctic Ocean climate system.

6. Conclusions

[36] The results in this paper add to the work of KR99. The multidecadal record of Fram Strait sea ice area flux, from passive microwave ice motion, now spans a period of 24 years. Between the 1980s and 1990s, the decadal difference in the net exported ice area is ~400,000 km^2, approximately half the annual average. The peak in the record, associated with an extreme in the NAO index, occurred in 1994/1995. Except for the years with extreme negative NAO, correlation of winter ice area export with the NAO index remains high (R^2 = 0.62). If the long term connection of ice flux to large-scale atmospheric forcing were stable, it would provide a proxy indicator of an important component of the overall Arctic Ocean sea ice mass balance since variability of this component has potential climate consequences. A number of investigators [*Hilmer and Jung*, 2000; *Vinje*, 2001] noted that the increased coherency between NAO index and ice area flux from 1978 may not be characteristic of the two time series over a longer period (e.g., 1950–2000), suggesting a more complex relationship. These identified associations are useful for the underlying mechanisms and as diagnostic tools for climate models. The average annual ice volume flux over the 8-year record is ~2218 km^3/yr (0.07 Sv). As is, the largest uncertainty in the volume flux remains in our lack of knowledge of the cross-strait thickness profile. The potential uncertainty in the VNK98 parameterization of the thickness profile may be significant as only moorings with limited longitudinal extent are used in its derivation.

[37] Assessment of the PMW ice motion with buoy displacement and SAR ice motion provides added confidence in our sea ice area flux estimates. The uncertainties in the PMW ice motion are consistently 4–6 km when compared with both buoy and SAR data sets. The 5 years of high-resolution SAR ice motion, even though limited by available temporal sampling, gives a good depiction of the spatial variability of the average ice motion profile across the Fram Strait, especially in the high gradient regions near the Greenland coast and near the ice edge. This helped validate the assumed profile, used by

KR99, with a high-velocity gradient within 40 km of the coast with zero motion at the coast of Greenland. In the absence of continuous coverage with higher-resolution SAR observations, PMW ice motion is an alternative for providing systematic observations, albeit with higher uncertainty, of the Fram Strait ice area flux. The higher-resolution PMW sensors on the AQUA and ADEOS-II platforms should also improve the data quality.

[38] The 5 years of near continuous coverage by RADARSAT provides a high-resolution view of the character of the ice cover of Fram Strait. The winter variability in terms of width of the ice stream, the compactness of the ice cover, and the coverage of first-year ice can be seen in the SAR imagery. The proximity of the locations of the ULS moorings to the ice edge or open ocean, seen in the SAR imagery, gives an indication of the possible influence of the ice edge processes on the observed ice thickness distribution at the moorings. If the influence is large in certain years, the thickness distributions may not be representative of that exported from the Arctic Ocean and care should be exercised in the interpretations of the observed trends and estimated ice flux. It is also clear from the imagery that current moorings provide inadequate sampling of the cross-strait profile of ice thickness. High-resolution imagery can provide a guide for placement of ULS moorings, if logistic difficulties were not of concern, for better sampling of the ice volume exported from the Arctic Ocean. Ideally, sequential SAR imagery is the best data set for monitoring ice flux because of its resolution and its relative insensitivity to atmospheric effects. Potentially, both the European ENVISAT and the future Canadian RADARSAT-2 SAR sensors have the imaging capability to fill the role of providing these observations.

[39] Our examination of the record of ULS thickness distributions shows variability that is potentially linked to a number of interesting factors. Most importantly the characteristics of the time series seem to be indicative of the thickness characteristics of source regions of the sea ice exported through the Fram Strait. Overall, the mean seasonal cycle of thickness trends of the MY thickness mode is consistent with basal ice growth and melt observed on a 3-m floe. The interannual variability of the seasonal cycle in the thickness of the MY mode is high and seems to be a potentially good indicator of the atmospheric and ocean conditions of the Arctic Ocean during those years. Over the ~9-year period shown here, there is a significant negative trend in the mean of the ULS ice thickness distributions and the mode of the MY ice thickness. Whether these trends are indicative of the thickness trends of the Arctic Ocean is examined, as the time-varying behavior of the monthly ULS thickness distributions can be related not only to the seasonal cycle in the basal growth and melt, but also to the magnitude and pattern of ice motion in the Arctic Ocean, and proximity of the ULS moorings to the ice edge. Unlike area flux, no immediate connection of the ice thickness to the AO or NAO is apparent. There could be a time lag between changes in atmospheric forcing and the observed thickness distribution in the Fram Strait. The complex coupling between these factors can perhaps be more effectively elucidated with simulations from an ice ocean model.

[40] **Acknowledgments.** The monthly ice thickness distributions from upward-looking sonar measurements are from the ACSYS Arctic sea ice thickness database at the Norwegian Polar Institute (http://www.npolar.no/ADACIT). NAO indices are that of the Climate Analysis Section, NCAR, Boulder, USA [*Hurrell*, 1995]. RADARSAT image data are provided by the Alaska SAR Facility, Fairbanks, Alaska. The SMMR and SSM/I brightness temperature and ice concentration fields are provided by World Data Center A for Glaciology/National Snow and Ice Data Center, University of Colorado, Boulder, Colorado. Buoy drift data are provided by the International Arctic Buoy Program. We wish to thank the reviewers for their valuable suggestions. This work was carried out at the Jet Propulsion Laboratory, California Institute of Technology, and was supported by the National Aeronautics and Space Administration and the National Science Foundation.

References

Aagaard, K., and E. Carmack (1989), The role of sea ice and other fresh water in the Arctic circulation, *J. Geophys. Res.*, *94*(C10), 14,485–14,498.

Björk, G., J. Söderkvist, P. Winsor, A. Nikolopoulos, and M. Steele (2002), Return of the cold halocline layer to the Amundsen Basin of the Arctic Ocean: Implications for the sea ice mass balance, *Geophys. Res. Lett.*, *29*(11), 1513, doi:10.1029/2001GL014157.

Boyd, T. J., M. Steele, R. D. Muench, and J. T. Gunn (2002), Partial recovery of the Arctic Ocean halocline, *Geophys. Res. Lett.*, *29*(14), 1657, doi:10.1029/2001GL014047.

Cavalieri, D. J. (2002), A link between Fram Strait sea ice export and atmospheric planetary wave phase, *Geophys. Res. Lett.*, *29*(12), 1614, doi:10.1029/2002GL014684.

Dickson, R. R., J. Meincke, S.-A. Malmberg, and A. J. Lee (1988), The "Great Salinity Anomaly" in the northern North Atlantic 1968–1982, *Prog. Oceanogr.*, *20*, 103–151.

Dickson, R. R., T. J. Osborn, J. W. Hurrell, J. Meincke, J. Blindheim, B. Adlandsvik, T. Vinje, G. Alekseev, W. Maslowski, and H. Cattle (2000), The Arctic Ocean response to the North Atlantic Oscillation, *J. Clim.*, *13*, 2671–2696.

Hilmer, M., and T. Jung (2000), Evidence for a recent change in the link between North Atlantic Oscillation and Arctic sea ice export, *Geophys. Res. Lett.*, *27*(7), 989–992.

Hurrell, J. W. (1995), Decadal trends in the North Atlantic Oscillation: Regional temperatures and precipitation, *Science*, *269*, 676–679.

Kwok, R., and G. F. Cunningham (2002), Seasonal ice area and volume production of the Arctic Ocean: November 1996 through April 1997, *J. Geophys. Res.*, *107*(C10), 8038, doi:10.1029/2000JC000469.

Kwok, R., and D. A. Rothrock (1999), Variability of Fram Strait Flux and North Atlantic Oscillation, *J. Geophys. Res.*, *104*(C3), 5177–5189.

Kwok, R., J. C. Curlander, R. McConnell, and S. Pang (1990), An ice motion tracking system at the Alaska SAR facility, *IEEE J. Oceanic Eng.*, *15*(1), 44–54.

Kwok, R., A. Schweiger, D. A. Rothrock, S. Pang, and C. Kottmeier (1998), Sea ice motion from satellite passive microwave data assessed with ERS and buoy motions, *J. Geophys. Res.*, *103*(C4), 8191–8214.

Lewis, E. L. (2000), Introduction, in *The Freshwater Budget of the Arctic Ocean*, edited by E. Lyn Lewis, pp. xv–xxi, Kluwer Acad., Norwell, Mass.

Martinson, D. G., and M. Steele (2001), Future of the Arctic sea ice cover: Implications of an Antarctic analog, *Geophys. Res. Lett.*, *28*(2), 307–310.

Rothrock, D. A., R. Kwok, and D. Groves (2000), Satellite views of the Arctic ocean freshwater balance, in *The Freshwater Budget of the Arctic Ocean*, edited by E. Lyn Lewis, pp. 409–452, Kluwer Acad., Norwell, Mass.

Steele, M., and T. Boyd (1998), Retreat of the cold halocline layer in the Arctic Ocean, *J. Geophys. Res.*, *102*(C5), 10,419–10,435.

Steele, M., and G. M. Flato (2000), Sea ice growth, melt, and modeling, in *The Freshwater Budget of the Arctic Ocean*, edited by E. Lyn Lewis, pp. 533–588, Kluwer Acad., Norwell, Mass.

Thompson, D. W. J., and J. M. Wallace (1998), The Arctic oscillation signature in the wintertime geopotential height and temperature grids, *Geophys. Res. Lett.*, *25*(9), 1297–1300.

Vinje, T. (2001), Fram Strait ice fluxes and atmospheric circulation: 1950–2000, *J. Clim.*, *14*, 3508–3517.

Vinje, T., N. Norland, and Å. Kvambekk (1998), Monitoring ice thickness in Fram Strait, *J. Geophys. Res.*, *103*(C5), 10,437–10,449.

G. F. Cunningham, R. Kwok, and S. S. Pang, Jet Propulsion Laboratory, California Institute of Technology, 4800 Oak Grove Drive, Pasadena, CA 91109, USA. (ron.kwok@jpl.nasa.gov)